https://doi.org/10.5194/hess-2021-362
Preprint. Discussion started: 13 July 2021

Hydrology and Earth System Sciences
Discussions

Stream discharge depends more on the temporal distribution of water inputs than on yearly snowfall fractions for a headwater catchment at the rain-snow transition zone

Leonie Kiewiet[1,2], Ernesto Trujillo[3,4], Andrew Hedrick[4], Scott Havens[4], Katherine Hale[5], Mark Seyfried[4], Stephanie Kampf[1], Sarah E. Godsey[2]

[1] Department of Ecosystem Science and Sustainability, Colorado State University, Fort Collins, CO, USA
[2] Department of Geosciences, Idaho State University, Pocatello, ID, USA
[3] Department of Geosciences, Boise State University, Boise, ID, USA
[4] USDA Agricultural Research Service, Boise, ID, USA
[5] Department of Geography, University of Colorado, Boulder, CO, USA

Abstract

Climate warming affects snowfall fractions and snowpack storage, displaces the rain-snow transition zone towards higher elevations, and impacts discharge timing and magnitude as well as low-flow patterns. However, it remains unknown how variations in the spatial and temporal distribution of precipitation at the rain-snow transition zone affect discharge. To investigate this, we used observations from eleven weather stations and snow depths measured in one aerial lidar survey to force a spatially distributed snowpack model (iSnobal/Automated Water Supply Model) in a semi-arid, 1.8 km^2 headwater catchment at the rain-snow transition zone. We focused on surface water inputs (SWI; the summation of rainfall and snowmelt) for four years with contrasting climatological conditions (wet, dry, rainy and snowy) and compared simulated SWI to measured discharge. We obtained a strong spatial agreement between snow depth from the lidar survey and model (r^2: 0.88), and a median Nash-Sutcliffe Efficiency (NSE) of 0.65 for simulated and measured snow depths for all modelled years (0.75 for normalized snow depths). The spatial pattern of SWI was consistent between the four years, with north-facing slopes producing 1.09 to 1.25 times more SWI than south-facing slopes, and snow drifts producing up to six times more SWI than the catchment average. We found that discharge in a snowy year was almost twice as high as in a rainy year, despite similar SWI. However, years with a lower snowfall fraction did not always have lower annual discharge nor earlier stream drying. Instead, we found that the dry-out date at the catchment outlet was positively correlated to the snowpack melt-out date. These results highlight the heterogeneity of SWI at the rain-snow transition zone and emphasize the need for spatially distributed modelling or monitoring of both the snowpack and rainfall.

Keywords: snowfall fraction, SWI, SWE, streamflow, dry-out date, non-perennial, satellite, iSnobal

1. Introduction

Due to increases in temperature, mountainous regions will receive less snow and more rain (Barnett et al., 2005; Stewart, 2009). This is concerning because snowmelt is a primary source for water resources across the globe (Barnett et al., 2005; Marks et al., 1999; Somers and McKenzie, 2020; Viviroli et al., 2007). On the scale of the continental United States (US), a decrease in the fraction of precipitation falling as snow (snowfall fraction hereinafter) is expected to decrease stream discharge (Berghuijs et al., 2014). However, lower snowfall fractions in much of the western United States have not yet led to a significant decrease in annual discharge (McCabe et al., 2017). Nonetheless, both observational data records (McCabe et al., 2017; Luce and Holden, 2009; Regonda et al., 2005) and future climate projections (Naz et al., 2016; Leung et al., 2004; Milly and Dunne,

https://doi.org/10.5194/hess-2021-362
Preprint. Discussion started: 13 July 2021

2020; Christensen et al., 2004) reveal earlier stream discharge peaks in response to earlier snowmelt, and a decline in summer low flows across the semi-arid mountainous US. One emerging question from these findings is how decreases in snowfall affect discharge in areas that already receive a mix of snow and rain.

The rain-snow transition zone is an elevation band within which the dominant phase of winter precipitation shifts between snow and rain (Nayak et al., 2010), and is often characterized by a transient snowpack in (at least) parts of the defined area. Multiple studies in the European Alps and the north-western United States have shown that snowfall fractions in lower and mid-altitude mountains, where the rain-snow transition zone is located, are particularly vulnerable to increases in temperature associated with climate change (Stewart, 2009). For example, the snowfall fraction in the Swiss Alps is projected to decrease between 50% (at ~2000 m) to 90% (~1000 m) towards the end of the century (Beniston et al., 2003). The current extent of the rain-snow transition zone covers about 9200 km^2 in the Pacific Northwest of the United States alone (here defined as Oregon, Washington, Idaho and the western part of Montana; Nolin and Daly, 2006), and is expanding and moving to higher elevations in response to climate change (Bavay et al., 2013; Nayak et al., 2010). This migration of the transition zone can affect precipitation patterns as well as discharge generation and timing across mountain ranges, with notable effects at the elevations surrounding the transition zone.

Climate change also has the potential to increase annual climate variations (Seager et al., 2012), affecting annual runoff efficiency (Hedrick et al., 2020) and likely also influencing stream discharge timing and magnitude. In mid-elevation rain-snow transition zones the annual snowpack variability is already relatively large. For example, in the Reynolds Creek Experimental Watershed (RCEW, in Idaho, US) the coefficient of variation (CV) of peak snow-water equivalent (SWE) between 1964 and 2006 ranged from 0.28-0.37 for five high-elevation stations (2056-2162 m) and was 0.72 for a mid-elevation weather station at the rain-snow transition zone (1743 m, Nayak et al., 2010). This mid-elevation variability suggests that year-to-year differences in snowfall at the rain-snow transition zone might already be substantial compared to nearby catchments at higher elevations. This allows the investigation of catchment responses to snowfall variations using a relatively short data record. One well-documented discharge response is that years in which catchments receive less snow have earlier snow-driven discharge peaks (McCabe and Clark, 2005; Stewart et al., 2005). Earlier spring snowmelt has been linked to an increased risk of wildfire for catchments across the western US (Westerling et al., 2006), as well as to earlier and lower low-flows (Kormos et al., 2016). In some catchments and years, portions of the stream network might also dry, altering the network's ecological and biogeochemical functioning (Datry et al., 2014). Using observations of hydro-climatically different years (e.g., rainy vs. snowy) could reveal how discharge and stream drying at the rain-snow transition zone has responded to past variations in water inputs, and thereby provide insight in how catchments might respond to future changes in rain/snow apportionments.

Annual or climate-driven variations in snowfall fractions might affect the spatial distribution of surface water inputs (SWI = rainfall + snowmelt). In years that receive less snow, the spatial pattern of SWI could depend more on the spatial distribution of rain, whereas the SWI pattern might reflect the distribution of the snowpack more strongly in years that receive more snow. In the semi-arid western US, rainfall magnitudes generally increase with elevation (Johnson and Hanson, 1995), whereas the spatial distribution of the snowpack is dependent on elevation, aspect, and wind-driven redistribution of snow, among other factors (Sturm, 2015; Tennant et al., 2017; Winstral and Marks, 2014; Trujillo et al., 2007). These primary controls on snow depth and SWE are relatively consistent from year to year, so the interannual distribution of snow is usually spatially consistent (Parr et al., 2020; Sturm, 2015; Winstral and Marks, 2002). The effects of elevation and aspect on the spatial distribution of snow depth, and thus, SWI, are well-studied in both high and mid-altitude mountains (e.g., Grünewald et al., 2014; López-Moreno and Stähli, 2008; Tennant et al., 2017), and the seasonal spatial distribution of SWI has been quantified at the rain-snow transition zone (Kormos et al., 2014). Snow drifting can also strongly impact the snowpack in the rain-snow transition zone, but thus far, research on snow drifting has been focused mainly on seasonally snow-covered areas (Mott et al., 2018), prairie and arctic environments (e.g., Fang and Pomeroy, 2009; Parr et al., 2020) or has been studied in the context of avalanches (e.g., Schweizer et al., 2003). These studies have shown that snow drifts can strongly influence the spatial water balance, that equator-facing slopes might only receive half as much SWI as areas that host snow drifts (Flerchinger and Cooley, 2000; Marshall et al., 2019), and that water originating from snow drifts can locally control groundwater level fluctuations (Flerchinger et al., 1992), and contribute to streamflow into the summer season (Chauvin et al., 2011; Hartman et al., 1999; Marks et al., 2002).

In addition to the spatial distribution of water inputs, the snowfall fraction also influences when SWI reaches the ground surface. Snowpacks store water and release snowmelt later, whereas rain on bare ground enters the hydrologic system instantaneously. After rainfall or snowmelt reaches the ground surface, it might become stream discharge, be stored in the soil, recharge deeper groundwater, or be evaporated or transpired. Generally, water inputs from rain or snowmelt during periods with high antecedent wetness and low evapotranspiration rates are more likely to recharge groundwater and generate discharge (Jasechko et al., 2014; Molotch et al., 2009; Hammond et al., 2019). However, rain and snowmelt inputs might result in similar runoff ratios (discharge/SWI) as long as the overall catchment wetness is similar or if the catchment is wet at key locations for water transport (Seyfried et al., 2009). The precipitation phase might also affect other hydrological processes that control water partitioning, for instance by inhibiting soil evaporation in areas that are snow-covered (Wang et al., 2013). Prevailing climatic conditions and subsurface storage capacity might also influence which route precipitation takes after it reaches the ground surface (Hammond et al., 2019), indicating that both the spatial and temporal distribution of SWI could affect if and when water reaches the stream.

Thus, our overarching goal is to improve our understanding of discharge response to year-to-year variations in precipitation phase and magnitude at the rain-snow transition zone - a region that covers a significant part of the land surface and might extend to higher elevations due to climate change. Specifically, we address the following research questions:

1. How does the spatial and temporal distribution of SWI at the rain-snow transition zone vary between particularly wet, dry, rainy or snowy years?

2. How does stream discharge respond to SWI in wet, dry, rainy or snowy years?

2. Site description

We focus our efforts in the Johnston Draw study area, a 1.8 km^2 headwater catchment at the Reynolds Creek Experimental Watershed (RCEW) in Idaho, USA. Elevations range from 1497 to 1869 m a.s.l., and mean annual air temperature and precipitation are 8.1 °C and 609 mm, respectively (2004-2014; Godsey et al., 2018). Previous research in RCEW has shown that mid-elevation catchments (1404 and 1743 m a.s.l.) have seen an increase in minimum daily temperatures (+0.57°C/decade), reduced snowfall (-32 mm/decade), and a decrease in streamflow (-0.75 x 10^6 m^3/decade) over the 1965-2006 data record, while there was no change in total precipitation (Nayak et al., 2010; Seyfried et al., 2011). The catchment is underlain by granite bedrock (79%), with some basalt (3%) and tuffs (18%) (Stephenson, 1970), and slightly deeper soils exist on the north-facing slopes, although the difference is not significant (1.31±0.56 m vs. 0.77±0.34 m, respectively, p-value: 0.05; Patton et al., 2019). Annual average soil water storage on the north-facing slopes is larger than on the south-facing slopes, which is largely due to the difference in soil depth and a later start of vegetation growth compared to the south-facing slopes (Godsey et al., 2018; Seyfried et al., in review). Snowberry (*Symphoricarpos*), big and low sagebrush (*Artemisia tridentate* and *Artemisia arbuscula*), aspen (*Populus tremuloides*) groves and wheatgrass (*Elymus trachycaulus*) characterize the north-facing slopes, whereas the south-facing slopes host *Elymus trachycaulus*, *Artemisia arbuscula*, mountain mahogany

https://doi.org/10.5194/hess-2021-362
Preprint. Discussion started: 13 July 2021

(*Cercocarpus ledifolius*) and bitterbrush (*Purshia tridentate*) (Godsey et al., 2018). Discharge at the catchment outlet is non-perennial, and the stream at the catchment outlet typically flows from early November until mid-July (MacNeille et al., 2020).

3. Methods

3.1 Hydrometeorological and discharge data

We used hourly hydrometeorological data recorded at eleven weather stations throughout the catchment (Fig. 1; Godsey et al., 2018). The stations are placed at 50-m elevation intervals on the north and south-facing slopes, and span a ~300 m elevation range (1508-1804 m a.s.l.; see Marks et al., 2013 for a detailed description). Observations started in 2002, although some stations were placed only in 2005 or 2010, and some were decommissioned in 2017 (see Godsey et al., 2018 for exact years). Air temperature, solar radiation, vapor pressure and snow depth were measured at hourly intervals at each of the stations, whereas additional measurements of wind speed, wind direction and precipitation were available at jdt125, jdt124, and jdt124b. The snow depth time series were processed to remove gaps and unreliable measurements during storms and smoothed over an 8-h window in most cases, and a 40-h window under specific circumstances (Godsey et al., 2018). Stream discharge data (Godsey et al., 2018) were obtained with a stage recorder using a drop box weir at the watershed outlet (Pierson et al., 2000). Stage height was converted to discharge using a stage height-discharge relationship (Pierson and Cram, 1998), and discharge was frequently measured by hand to ensure high data quality (Pierson et al., 2000).

3.2 Remotely sensed observations

To characterize the spatial distribution of snow depth, a 1-m resolution snow depth product was calculated as the difference between a snow-off LiDAR flight (10-18 November 2007; Shrestha and Glenn, 2016) and a snow-on LiDAR flight (18 March 2009, around the time of peak accumulation), hereafter referred to as lidar snow depth. Typical vertical accuracies for lidar surveys are ~10 cm (Deems et al., 2013). We assumed that uncertainties in both lidar surveys were uncorrelated, resulting in an overall uncertainty of ~14 cm for lidar snow depth (summation in quadrature). All pixels that yielded a negative snow depth were excluded. The lidar snow depths were higher than the weather station snow depths, but this pattern was consistent across the catchment resulting in a strong linear relation between the two individual sets of snow depth measurements (R^2: 0.88, Supplement S1).

Because we had only one lidar observation near peak snow accumulation, we also characterized snow presence throughout the season by mapping the snow-covered area (SCA) using satellite-derived surface reflectance at 3-m resolution, which is available starting in 2016 (4-band PlanetScope Scene; Planet Team, 2018). This high-resolution imagery was critical for our analysis because snow drifts in the rain-snow transition are relatively small in extent. Although no high-resolution satellite imagery was available for years that exhibited the key characteristics we sought to study (e.g., rainy, snowy, wet or dry; see section 3.3), we focused on the most recent snow-covered period for which streamflow data and Planet imagery were available (1 November 2018 until 31 May 2019) to assess snow coverage. We manually selected all available images in which the entire watershed was captured and for which snow was visually recognizable, then removed all images for which clouds significantly covered the watershed, resulting in 41 usable images. The information from all four spectral bands was then condensed to one layer using a principal component analysis (‘RSToolbox’ package in R). We used the Maximum Likelihood Classification tool in ArcGIS (Esri Inc., 2020) to identify the SCA, after manually training the tool by selecting areas with and without snow cover (average of 26895 pixels per class; median: 9019), visually aided by the original satellite imagery. Obtaining training data was most challenging during periods in which almost the entire area was snow-free or snow-covered, for densely vegetated areas, and when part of the catchment was shaded. To overcome the latter, we classified “snow-free”, “snow-covered”, and "shaded snow", in heavily shaded images, and afterwards merged "snow-covered" and "shaded snow". The mean confidence for all classifications is shown in Supplement S2. Our method differs from other satellite-derived snow products that combine both visible and infrared light, but yielded a higher resolution data product (3-m resolution vs. 30-m for Landsat-8 or 500-m for MODIS) that was necessary to capture the snow drifts in the rain-snow transition zone.

We also used the surface reflectance imagery to determine the melt-out date of the snowpack for all years in which satellite and discharge observations were available (2016-2019). This was done by manually reviewing all available images and visually determining when all snow had melted. Given the high visiting frequency and limited cloudiness in early summer, we estimate an error of ~2 days is appropriate for these melt-out dates.

3.3 Spatially distributed snowpack modelling

We used the Automated Water Supply Model (AWSM; Havens et al., 2020) to obtain a spatially continuous estimation of the distribution and phase of precipitation, snowpack characteristics and surface water inputs (SWI). The two major components of AWSM are the Spatial Modeling for Resources Framework (SMRF; Havens et al., 2017) and iSnobal (Marks et al., 1999). iSnobal is a physically-based, two-layer snowpack model that accounts for precipitation advection from rain and snow (Marks et al., 1999). We used SMRF to spatially distribute precipitation and all other weather variables (air temperature, solar radiation, vapor pressure, precipitation, wind speed and wind direction) along an elevation gradient using the hourly measurements from the weather stations. We included precipitation measurements from two stations within the basin (jdt125 and jdt124b) and two stations outside of the basin (jd144 and jd153, Fig. 1) to capture the elevation gradient. Precipitation at wind-exposed site jdt124 was excluded because of precipitation undercatch issues. The interpolated vapor pressure and temperature fields were then used within SMRF to calculate the dew point, and further distinguish which fraction of precipitation falls as rain and/or snow. The model was run at a 10-m resolution for five water years, namely, 2005, 2009, 2010, 2011 and 2014. We selected 2009 because the snow depth lidar survey was available in this year, and 2005, 2010, 2011 and 2014 because they provide a representation of rainy, snowy, dry and wet conditions, respectively (Table 1). We focus on the latter four years in the results and discussion of this manuscript but evaluate the model performance for all years.

In order to represent the spatial variability in snowfall and the effects of wind redistribution of snow, we use the precipitation rescaling approach proposed by Vögeli et al. (2016) that implicitly captures the spatial heterogeneity induced by these processes using distributed snow depth information (e.g., from lidar or structure from motion (SfM)). This methodology can be used to rescale the precipitation falling as snow to reproduce the observed snow distribution patterns while conserving the initial mass estimation. Given the inter- and intra-annual consistency of spatial patterns of snow distribution (Pflug and Lundquist, 2020; Schirmer et al., 2011; Sturm and Wagener, 2010), Trujillo et al. (2019, manuscript in preparation) has been extending the original implementation to utilize historical snow distribution information to other years in the iSnobal model. Following these successful implementations, we use the spatial distribution of snow depth from the 2009 survey around peak snow accumulation to inform the snowfall rescaling to all years in the study period. Although using the 2009 survey to rescale snowfall in other years might have induced some uncertainty, this uncertainty is likely to be small given the intra-annual consistency in snow distribution patterns, which was verified in this catchment by comparing the lidar snow depth and the satellite imagery.

3.4 SWI

One of the model outputs from iSnobal is 'surface water inputs' (SWI), which represents snowmelt from the bottom of the snowpack, rain on bare ground, or rain percolating through the snowpack. iSnobal is limited to surface processes only, which

https://doi.org/10.5194/hess-2021-362
Preprint. Discussion started: 13 July 2021

means that SWI 'exits' the modelling domain. In reality, SWI might travel to the stream as surface or subsurface runoff, could be stored in the soil until it evaporates or is transpired, or could recharge deeper groundwater storages. The route that SWI takes depends on the overall catchment wetness as well as the local energy balance (e.g., incoming radiation) and vegetation activity. In this manuscript, we computed SWI for each pixel and time step and assumed that all SWI generated in simulated snow-free pixels was rain and that all SWI generated in simulated snow-covered pixels was snowmelt.

3.5 Model evaluation

Model results were evaluated in two ways. First, the simulated snow depths were compared to lidar snow depths covering the entire basin on March 18, 2009; and second, the temporal variation of the simulated snow depths were compared to snow depths measured at each of the weather stations for all simulated years. The latter comparison was done using model results from a 30-m x 30-m area surrounding each station; this is equivalent to 3x3 grid cells because the model was run at a 10-m resolution. We computed the Root Mean Square Error (RMSE) and Nash-Sutcliffe Efficiency (NSE; Nash and Sutcliffe, 1970) for the observed versus simulated snow depths, as well as the NSE for the normalized observed versus normalized simulated snow depths (NSE_{norm}). NSE_{norm} reflects the ability of the model to reproduce the dynamic behaviour of the snowpack.

4. Results

4.1 Snow depth observations

The lidar snow depth ranged from 0 to 5.3 m on the date of acquisition (18 March 2009), which was near peak snow cover (median: 0.4 m; CV: 0.91; Fig. 2a). The south-facing slopes had little to no snow cover (mean: 0.3 m), whereas the north-facing slopes were covered with 0.7 m of snow on average. For the years studied here, during the approximate duration of the snowy season between 15 Nov and 15 Apr, the average snow depth for all north-facing stations was more than five times that of the average snow depth at south-facing stations (20.2 vs. 3.7 cm, respectively), and the snowpack lasted almost 90 days longer on average (132 vs. 43 days, respectively). Although weather stations on north-facing slopes and at higher elevations generally had deeper snowpacks and were snow-covered longer than sites on the south-facing slopes or at lower elevations (data not shown), this pattern was masked by the effects of other processes. For instance, snow depths at jdt2 (north-facing) and jdt3b (south-facing) were consistently lower than at the weather stations directly below them in elevation (jdt1 and jdt2b, respectively). Large snow drifts formed in some western parts of the watershed, up to a maximum depth of 5.3 m (90^{th} percentile of all snow depths = 1.2 m, Fig. 2a). Wind-driven redistribution of the snow in Johnston Draw is facilitated by a relatively consistent southwestern wind direction (average during storms: 225°), and high wind speeds (average during storms at wind-exposed station jdt124: 6.7 m s^{-1}; Godsey et al., 2018).

4.2 Model performance in space and over time

Simulated snow depths on the day of the lidar survey agreed well with the lidar snow depth (r^2: 0.88, Fig. 2a-c). The residual snow depths (lidar – simulation) were approximately normally distributed, with a mean of 0.2 m (see Supplement S3 for a histogram and QQ plot). The largest differences (maximum difference: 1.1 m) between the simulated and measured snowpack were for isolated 10 m pixels on both the north- and south-facing slopes (Fig. 2c). The spatial pattern of the lidar snow depth also agreed well with the spatial patterns of snow-covered area (Fig. 2a,d), and there was a strong agreement between the simulated snow-covered area for 2009 (Fig. 2e) and the snow-covered area determined from satellite imagery for 2019 (Fig. 2d). This indicates that the model captured the spatial distribution of the snowpack as well as the differential melt-out patterns, and that the location of the snow drifts was consistent between 2009 and 2019.

https://doi.org/10.5194/hess-2021-362
Preprint. Discussion started: 13 July 2021

The median NSE for the hourly simulated snow depths compared to observations at the weather stations ranged from 0.22 (wet 2011) to 0.86 (snowy 2010) for all modelled years and weather stations, with RMSE ranging from 0.8 to 9.7 cm (Table 2, see Supplement S4 for time series of all simulated and observed snow depths). RMSE was lower than 10 cm for all years, with the year in which the NSE performance was lowest (wet 2011) having an RMSE of 4.6 cm. There were no weather stations for which the model performed consistently poor or well, with both high and low NSE values at each of the stations (e.g., range NSE at jdt4: -9.60 to 0.91 and jdt1: 0.01 to 0.83). The temporal variation of the snowpack at each of the weather stations was well-captured by the model; the median NSE for the normalized snowpack depths (NSE_{norm}) ranged from 0.65 to 0.94 (median: 0.75), although there were some sites and years with low NSE (Table 2). This indicates that the overall patterns of snow accumulation and melt were captured by the model and implies that the temporal distribution of snow-covered area (SCA) and surface water inputs (SWI) simulated by the model are reliable.

4.3 Spatial and temporal pattern of surface water inputs (SWI)

The spatial pattern of SWI was similar for all years, with the highest SWI in areas hosting snow drifts (maximum SWI (SWI_{max}): 3892 mm; 98th percentile of SWI (SWI_{98}): 1235 mm, both in wet 2011; Fig. 3, Table 1). Annual SWI across the rest of the catchment varied less, with north-facing slopes receiving 45 to 127 mm more SWI than south-facing slopes (values for rainy 2005 and snowy 2010, respectively; Table 1). Areas hosting snow drifts received 1.7 to 2.7 times more SWI than the catchment average (ratio SWI_{98}/SWI_{avg}). Summarizing SWI by aspect (see polar diagrams in Fig. 3) revealed the highest SWI on northeast-facing slopes and roughly equal annual SWI for all other aspects. Differences between the northeast-facing slopes and other parts of the catchment were largest in snowy 2010 (ratio of major/minor axis of polar plot: 1.29), and smallest in rainy 2005 and dry 2014 (ratio: 1.13 and 1.17, respectively).

Weekly sums of SWI ranged from 0 to ~75 mm in all years (Fig. 4). Summer most frequently had weeks without SWI generation, whereas the highest weekly SWI occurred with simultaneous rainfall and snowmelt (i.e., rain-on-snow events, as for instance in February 2014, Fig. 4d). However, large rainfall events without snowfall or snow cover in spring of rainy 2005 (weekly SWI: ~75 mm), and in fall of wet 2011 (weekly SWI: ~50 mm; grey peaks in Fig. 4a and c) also generated high SWI. In 2011, the majority of SWI was generated in winter and spring (47% between December and May, see inset in Fig. 4c) whereas in dry 2014 most SWI was generated in winter (54% between December and February, Fig. 4d). In 2005 and 2010 most SWI was generated in spring (March-May 32% and 46%, respectively). Although similar amounts of SWI occurred in spring in 2005 and 2010 (339 and 388 mm, respectively), in 2005 93% came from rain, whereas in 2010 only 35% came from rain. As a result, average daily SWI rates were higher in snowy 2010 than in rainy 2005 (mean SWI rate March-May: 3.7 mm d^{-1} in 2010 vs. 2.9 mm d^{-1} in 2005). Overall, variations in weekly and daily SWI rates were lower in 2010 (CV daily SWI: 1.71) than in all other years (2.50 in 2005, 2.14 in 2011, and 2.65 in 2014).

4.4 Stream discharge

Streamflow was least responsive to SWI at the beginning of each water year (Fig. 5). For instance, in 2005 and 2010, 174 and 108 mm of SWI occurred before February 1st (31% and 20% of annual SWI), whereas discharge amounted to only 7% and 1% of its yearly total during that same period. Similarly, 82 mm of SWI in October 2011 resulted in less than 1 mm discharge, whereas roughly 30% of SWI left the catchment via the stream in the following period (Nov-Jan SWI: 180 mm, discharge: 62 mm). After the wet-up period, SWI resulted in most discharge when SWI rates were high, such as during a 3-day rain-on-snow event in February 2014 (SWI: 75 mm, discharge: 29 mm) or during spring snowmelt in April 2011 (SWI: 108 mm, discharge: 102 mm).

Annual discharge was highest in 2011 (307 mm, 43% of SWI) and lowest in 2005 (62 mm, 11% of SWI). Despite similar SWI inputs in 2005 and 2010 (SWI_{avg}: 553 and 557 mm, respectively, Table 1), snowy 2010 had nearly twice as much annual discharge as rainy 2005 (117 mm, 21% of SWI). Apart from these two years, there was no relation between annual discharge and the annual snowfall fraction (Fig. 6c), nor between annual discharge and the amount of SWI coming in as rain or snow in different seasons (winter, spring, summer, or any combination of these periods). By considering additional years (for which SWI was not simulated), we found that annual discharge was positively related to the amount of precipitation recorded at the lowest precipitation station (jdt125, r^2=0.80, Fig. 6a). Annual discharge was slightly higher for years that were preceded by a year that received above average annual precipitation (see Supplement S6), but the correlation coefficient decreased when including the precipitation totals recorded in the preceding year (e.g., annual discharge vs. precipitation in the same year + 0.5 times precipitation previous year, S6). This indicates that any memory effect is likely to be small in this catchment.

Except for wet 2011, the annual runoff efficiency (discharge/SWI) was higher for years that had a lower average weekly SWI rate (annual SWI/number of weeks in which SWI was generated). Although the temporal distribution of SWI is affected by the phase of precipitation (Fig. 4), average weekly SWI rates were not related to the annual snowfall fraction (r^2: 0.06). Individual precipitation events also had a strong influence on the annual runoff efficiency. For instance, dry 2014 had a higher runoff efficiency (0.16) than 2005 (0.11) and 2009 (0.14), but this was mostly due to the high runoff generation during one rain-on-snow event (29 mm, 36% of yearly discharge).

Stream drying occurred in each of the five years except 2011 (Table 1, Fig. 5). The stream dried earliest in 2014 (13 July), and in late August in 2009, 2005 and 2010 (Table 1). For the five years studied here, the stream dry-out date (the first day at which discharge equals zero) was later for years receiving more SWI (r^2: 0.84), and for years that had a later melt-out date (date at which all snow had melted; r^2: 0.77 for all coloured points in Fig. 6b). When considering the melt-out dates for four additional years based on planet-lab satellite observations (2016-2019, section 3.2), we found that the dry-out date was later in years when snow persisted longer (r^2: 0.54 for all points in Fig. 6b). There was no relation between the annual snowfall fraction and the stream dry-out date (Fig. 6d).

5. Discussion

Spatial variability in SWI

Snow drifting and aspect-driven differences in snow dynamics caused a strong variability in the spatial pattern of the snowpack (Fig. 2a) and SWI (Fig. 3). We found that the spatial pattern in SWI was similar across all years, with snow drifts receiving up to seven times more SWI than the catchment average (SWI_{max}/SWI_{avg} in 2010, Table 1). Even in rainy 2005, SWI was more than 3.5 times higher in the snow drifts (SWI_{max}: 2005 mm) compared to the catchment average (SWI_{avg}: 573 mm, Table 1). In our modelling routine, the spatial consistency between years is pre-determined by the snowfall rescaling (see section 3.3), but this likely also reflects real-world conditions, as the spatial agreement between the independently collected satellite imagery and lidar snow depths suggests (Fig. 2). Most importantly, the nearly four-fold variation in SWI over less than a kilometre distance is equivalent to the average precipitation difference between most of Reynolds Creek and the peaks of the Cascade Mountains in Oregon, or shifting from semi-arid steppe to coastal mountain snowpacks, and directly affects water-limited processes such as weathering or the plant species distribution. One local example of this are the aspen stands which are uniquely located directly below the snow drifts (Kretchun et al., 2020), while sagebrush is predominant in the rest of the catchment. Because snow drifts drive the spatial pattern of SWI, it is crucial to quantify wind-driven redistribution processes as well as capture aspect and elevation-driven processes, even at the rain-snow transition zone.

Snow drifts delivered 4.2% (2005) to 7.2% (2010) of the basin-total annual SWI on just ~2% of the land surface, and persisted longer, compared to non-drift areas, into the spring season (Fig. 3d-e). Previous work in the seasonally snow-covered Reynolds Mountain East catchment, showed that snow drifts indeed hold a large fraction of total catchment snow water equivalent (SWE), with 50% of total SWE on just 31% of the catchment area (Marks et al., 2002), and SWI varying strongly in space, ranging from 150 to 1100 mm for individual grid cells (10 – 20 m) in the relatively dry water year 2003 (Seyfried et al., 2009). Snow drifts in Johnston Draw are shallower (up to 5 m in 2009) and covered a smaller portion of the area (~2%) than in the higher elevation Reynolds Mountain East catchment, but are proportionally even more important in the rain-snow transition zone by hosting up to 15% of SWE during peak SWE in snowy 2010 and 25% in rainy 2005. Water originating from snow drifts has been shown to locally control groundwater level fluctuations (Flerchinger et al., 1992), and contribute to streamflow into the summer season (Chauvin et al., 2011; Hartman et al., 1999; Marks et al., 2002). For instance, in the Upper Sheep Creek watershed, also in RCEW, Chauvin et al. (2011) showed that the lowest stream discharge was recorded for the year in which snow drifts were least prominent. In Johnston Draw, the stream dry-out date was positively correlated with the drift melt-out date (Fig. 6), suggesting that isolated snow patches are also important for sustaining streamflow. These results do not reveal the mechanism or influence of the specific drift location since neither subsurface flow nor streamflow generation processes were measured or simulated. Nonetheless, observations of snow drifts from satellite imagery are consistent with model simulations of SCA (Fig. 2 and 6) and are easily obtained from high-resolution imagery. This suggests that satellite observations might be an alternative information source to predict stream drying in drift-influenced watersheds.

Temporal variability in SWI and discharge response

We found that the majority of SWI occurred in winter and spring, and that catchment-average SWI was more uniform in time in snowy 2010 than in the other years (CV of daily SWI, 2010: 1.7; other years: 2.14 – 2.65). We hypothesize that the steadier water inputs in that year might explain why annual discharge in snowy 2010 was double that of rainy 2005 despite similar precipitation. More stable water inputs from snowmelt rather than flashy water inputs from rain could have led to wetter soils and higher soil conductivity rates, allowing more water to pass through the subsurface towards the stream or towards deeper storages (Hammond et al., 2019). Previous work in the nearby Dry Creek Experimental Watershed (Idaho) showed that water stored in the soil dries out approximately ten days after snowmelt (McNamara et al., 2005). For the years on record here, streamflow was sustained for a minimum of 59 days after the melt-out date (Table 1), while SWI during this period was generally low (Fig. 4). This underscores that it is indeed likely that deeper flow paths contributed to the stream in the early summer. This is also consistent with stream discharge being nearly unresponsive to SWI during the dry catchment conditions in the beginning of each water year (Fig. 5). During fall, subsurface water storage across the catchment is low, and any SWI during this period thus likely results in recharge rather than stream discharge (Seyfried et al., in review). Alternatively, SWI during early fall might be used to satisfy evaporative demands. In any case, further simulations are required to fully understand how precipitation amounts, timing and location interact with subsurface water storage to control stream discharge.

In contrast to our hypothesis and what has been suggested in the literature (e.g., based on the comparison of 420 catchments in the continental US using the Budyko framework, Berghuijs et al., 2014), neither annual discharge nor the stream dry out-date were correlated with snowfall fraction (Fig. 6). Instead, total precipitation and the snowpack melt-out date were positively related to annual discharge and the stream dry-out date. This highlights the importance of the temporal distribution of SWI, which is not captured in an annual value for snowfall. The temporal distribution of SWI might be less important for predicting stream discharge and cessation in more humid catchments in which precipitation is more evenly distributed over the year and/or in which more events occur, or in larger catchments, such as those considered in Berghuijs et al., (2014; range catchment areas: 67-10,329 km^2). We found that individual precipitation events can also heavily influence the yearly runoff efficiency, as described for 2014 (section 4.4). As such, considering inter-annual variability and events is an important addition to annual average values, when investigating how precipitation affects discharge in semi-arid regions.

Bilish et al. (2020) similarly found that streamflow was not correlated to the snowfall fraction for a small catchment with an ephemeral snowpack in the Australian Alps. They attributed this to the frequent occurrence of mid-winter snowmelt; the snowpack melted out several times each year, independent of the annual snowfall fraction, and the snowpack thus did not store a significant amount of water. Field observations at Dry Creek, a nearby semi-arid catchment that includes a rain-dominated and a snow-dominated area, also suggested that the snowfall fraction was not related to annual discharge for a small catchment at the rain-snow transition zone (Treeline catchment, 0.015 km^2), but a relation did exist when considering the entire Dry Creek catchment (28 km^2, J. McNamara, personal communication). Another study at Dry Creek suggested that the snowfall fraction is less important than spring precipitation for sustaining upland ecosystems (McNamara et al., 2005), emphasizing the importance of the temporal distribution of SWI for other semi-arid catchments. For the years studied here, we did not find a relation between stream drying and spring precipitation, but our findings do corroborate that streamflow is more sensitive to total precipitation than to snowfall fraction (Fig. 6).

Limitations and opportunities

Though the model adequately reproduced the spatial snowpack patterns and dynamics (Fig. 3 and Table 2), temporal variations in the snow depths (i.e., melt and accumulation) recorded at the weather station locations were simulated better than the absolute snow depths. We suggest three reasons for the differences between simulated and observed snow depths. First, there was uncertainty in the precipitation measurements and the spatial distribution thereof. Precipitation was interpolated based on elevation, after which the proportion of precipitation falling as snow was redistributed based on the lidar snow depths (see section 3.3). Uncertainties in either data products or in the spatial extrapolation thereof will have decreased the model efficiency. Second, the simulated snow depths reflect all processes occurring in each 10-m grid cell (our model resolution), whereas the ultrasonic snow depth measurements represent processes at ~1-3 m^2. Small differences between the simulated and observed snow depths are therefore expected. Third, iSnobal is a mass and energy balance model, and therefore optimized to correctly model mass. Model evaluation using snow depths (instead of SWE) is thus less favourable, since small differences in snow densities and SWE could lead to significant differences in snow depths. However, since snow depth measurements were available and SWE measurements were not, we focused on snow depth. Uncertainties were also present in the weather station snow depths, as well as the lidar-based snow depths and the satellite-based SCA analysis. We compared the spatial patterns from the lidar and satellite imagery to test if the spatial pattern was consistent between these two data sources and found this to be the case (Fig. 2). As such, we are confident that despite the uncertainties of our analysis, we captured the within-catchment variability of the snowpack and also adequately modelled the variability in SWI that we set out to investigate.

Discrepancies between simulated and observed snow depths are challenging to solve, especially for areas with an ephemeral snow cover (Kormos et al., 2014) or with complex vegetation patterns, such as the sagebrush in Johnston Draw. Shallow snow covers are more sensitive to small variations in energy fluxes than deeper seasonal snow covers (Pomeroy et al., 2003; Williams et al., 2009). As a result, small errors in the spatial extrapolation of the forcing data or in the forcing data itself (e.g., uncertainty in the observed relative humidity or temperature) can result in large uncertainties in the model results (Kormos et al., 2014). For instance, the transition from snow-covered to snow-free areas results in a large change in albedo, which influences solar radiative fluxes. The snowpack at the rain-snow transition zone can melt out several times per year, even within a single day, and melt-out dates are variable across the catchment. Therefore, a small error in the simulated melt-out date for each cell can result in a larger error in the basin-average or yearly results. Perhaps these challenges are also a reason for the limited number of studies that have simulated warm snowpacks (Kormos et al., 2014; Kelleners et al., 2010), despite multiple regional studies highlighting that the rain-snow transition zone is expanding and that their climates are changing rapidly (Klos et al., 2014; Nolin and Daly, 2006). Challenges linked to snow ephemerality likely also affected our results, but the agreement between the observed and simulated snow depths indicates that at least the general patterns of accumulation and melt in space and over time were represented by the simulations, at a scale that was small enough to characterize the snow drifts.

Regardless of the challenges that come with studying an intermittent snow cover, the relationship between the snowpack melt-out date and stream dry-out date poses interesting opportunities to inform hydrological models or evaluate model results with independent observations. Measurements of SCA can be obtained through satellite imagery and are thus easier and cheaper to obtain than SWE or snow depth measurements (e.g., Elder et al., 1991). Satellite observations can be particularly helpful to investigate remote areas that exceed a feasible modelling domain, and can be used to inform or evaluate models. Given the restrictions for satellite imagery imposed by clouds and visit-frequency, particularly for areas with an ephemeral snow cover that might melt out in a single day, a combination of satellite imagery and snowpack modelling seems a promising way to leverage these observations while ensuring the fine temporal resolution that might be needed to study stream cessation.

6. Conclusions

As a result of climate change, the rain-snow transition zone will receive more rain and less snow, which influences the spatial and temporal distribution of surface water inputs (SWI, summation of rainfall and snowmelt). The goal of this work was to quantify the spatial and temporal distribution of SWI at the rain-snow transition zone, and to assess the sensitivity of stream discharge to the temporal distribution of SWI as well as to the annual snowfall fraction. To this end, we used a spatially distributed snowpack model to simulate SWI during five years, of which four had contrasting climatological conditions. We found that the spatial pattern of SWI was similar between years, and that snow drifting and aspect-controlled processes caused large differences in SWI across the watershed. Some areas received up to six times more SWI than other sites, and the difference between SWI from the snow drifts and catchment average SWI was highest for the year with the highest snowfall fraction. The majority of SWI occurred in winter or spring, which was also the time that the percentage of SWI becoming streamflow was highest (up to 94% in April 2011). Despite similar annual SWI (553 vs. 557 mm) and a similar timing of SWI (majority of SWI in spring), snowy 2010 had about twice as much stream discharge as rainy 2005. However, in contrast to our hypothesis, years with a lower snowfall fraction did not always have lower discharge nor earlier stream drying in summer. This highlights the potential importance of where SWI reaches the ground surface, in addition to when and how much SWI occurs. We found that the dry-out date at the catchment outlet was positively correlated to the last day at which there was snow present anywhere in the catchment. These results highlight the heterogeneity of SWI at the rain-snow transition zone and its impact on stream discharge, and thus the need for spatially and temporally representing SWI in headwater-scale studies that simulate streamflow.

Data availability

The hydrometeorological and discharge data used in this paper is available via Godsey et al. (2018), satellite imagery can be obtained via Planet Team (2018) and remaining data is available upon reasonable request.

Author contribution

LK developed the concept of the study together with SEG. LK, SH, ET, AH and KH performed and/or contributed to the simulations. LK prepared the first draft of the manuscript. All co-authors provided recommendations for the data analysis, participated in discussions about the results, and edited the manuscript.

Competing interests

The authors declare that they have no conflict of interest.

Financial support

This research has been supported by the Swiss National Science Foundation (grant no. P2ZHP2_191376).

Bibliography

Barnett, T. P., Adam, J. C., and Lettenmaier, D. P.: Potential impacts of a warming climate on water availability in snow-dominated regions, Nature, 438, 303–309, https://doi.org/10.1038/nature04141, 2005.

Bavay, M., Grünewald, T., and Lehning, M.: Response of snow cover and runoff to climate change in high Alpine catchments of Eastern Switzerland, Adv. Water Resour., 55, 4–16, https://doi.org/10.1016/j.advwatres.2012.12.009, 2013.

Beniston, M., Keller, F., Koffi, B., and Goyette, S.: Estimates of snow accumulation and volume in the Swiss Alps under changing climatic conditions, Theor. Appl. Climatol., 76, 125–140, https://doi.org/10.1007/s00704-003-0016-5, 2003.

Berghuijs, W. R., Woods, R. A., and Hrachowitz, M.: A precipitation shift from snow towards rain leads to a decrease in streamflow, Nature Clim. Change, 4, 583–586, https://doi.org/10.1038/nclimate2246, 2014.

Bilish, S. P., Callow, J. N., and McGowan, H. A.: Streamflow variability and the role of snowmelt in a marginal snow environment, Arct. Antarct. Alp. Res., 52, 161–176, https://doi.org/10.1080/15230430.2020.1746517, 2020.

Chauvin, G. M., Flerchinger, G. N., Link, T. E., Marks, D., Winstral, A. H., and Seyfried, M. S.: Long-term water balance and conceptual model of a semi-arid mountainous catchment, J. Hydrol., 400, 133–143, https://doi.org/10.1016/j.jhydrol.2011.01.031, 2011.

Christensen, N. S., Wood, A. W., Voisin, N., Lettenmaier, D. P., and Palmer, R. N.: The Effects of Climate Change on the Hydrology and Water Resources of the Colorado River Basin, Climatic Change, 62, 337–363, https://doi.org/10.1023/B:CLIM.0000013684.13621.1f, 2004.

Datry, T., Larned, S. T., and Tockner, K.: Intermittent Rivers: A Challenge for Freshwater Ecology, BioScience, 64, 229–235, https://doi.org/10.1093/biosci/bit027, 2014.

Deems, J. S., Painter, T. H., and Finnegan, D. C.: Lidar measurement of snow depth: a review, J. Glaciol., 59, 467–479, https://doi.org/10.3189/2013JoG12J154, 2013.

Elder, K., Dozier, J., and Michaelsen, J.: Snow accumulation and distribution in an Alpine Watershed, Water Resour. Res., 27, 1541–1552, https://doi.org/10.1029/91WR00506, 1991.

Esri Inc.: ArcMap (version 10.7.1), 2020.

https://doi.org/10.5194/hess-2021-362
Preprint. Discussion started: 13 July 2021

Hydrology and Earth System Sciences Discussions

Fang, X. and Pomeroy, J. W.: Modelling blowing snow redistribution to prairie wetlands, Hydrol. Process., 23, 2557–2569, https://doi.org/10.1002/hyp.7348, 2009.

Flerchinger, G. N. and Cooley, K. R.: A ten-year water balance of a mountainous semi-arid watershed, J. Hydrol., 237, 86–99, https://doi.org/10.1016/S0022-1694(00)00299-7, 2000.

Flerchinger, G. N., Cooley, K. R., and Ralston, D. R.: Groundwater response to snowmelt in a mountainous watershed, J. Hydrol., 133, 293–311, https://doi.org/10.1016/0022-1694(93)90146-Z, 1992.

Godsey, S. E., Marks, D., Kormos, P. R., Seyfried, M. S., Enslin, C. L., Winstral, A. H., McNamara, J. P., and Link, T. E.: Eleven years of mountain weather, snow, soil moisture and streamflow data from the rain–snow transition zone – the Johnston Draw catchment, Reynolds Creek Experimental Watershed and Critical Zone Observatory, USA, Earth Syst. Sci. Data, 10, 2018.

Grünewald, T., Bühler, Y., and Lehning, M.: Elevation dependency of mountain snow depth, Cryosphere, 8, 2381–2394, https://doi.org/10.5194/tc-8-2381-2014, 2014.

Hammond, J. C., Harpold, A. A., Weiss, S., and Kampf, S. K.: Partitioning snowmelt and rainfall in the critical zone: effects of climate type and soil properties, Hydrol. Earth Syst. Sci., 23, 3553–3570, https://doi.org/10.5194/hess-23-3553-2019, 2019.

Hartman, M. D., Baron, J. S., Lammers, R. B., Cline, D. W., Band, L. E., Liston, G. E., and Tague, C.: Simulations of snow distribution and hydrology in a mountain basin, Water Resour. Res., 35, 1587–1603, https://doi.org/10.1029/1998WR900096, 1999.

Havens, S., Marks, D., Kormos, P., and Hedrick, A.: Spatial Modeling for Resources Framework (SMRF): A modular framework for developing spatial forcing data for snow modeling in mountain basins, Comput. and Geosci., 109, 295–304, https://doi.org/10.1016/j.cageo.2017.08.016, 2017.

Havens, S., Marks, D., Sandusky, M., Hedrick, A., Johnson, M., Robertson, M., and Trujillo, E.: Automated Water Supply Model (AWSM): Streamlining and standardizing application of a physically based snow model for water resources and reproducible science, Comput. and Geosci., 144, 104571, https://doi.org/10.1016/j.cageo.2020.104571, 2020.

Hedrick, A. R., Marks, D., Marshall, H., McNamara, J., Havens, S., Trujillo, E., Sandusky, M., Robertson, M., Johnson, M., Bormann, K. J., and Painter, T. H.: From Drought to Flood: A Water Balance Analysis of the Tuolumne River Basin during Extreme Conditions (2015 – 2017), Hydrological Processes, hyp.13749, https://doi.org/10.1002/hyp.13749, 2020.

Jasechko, S., Birks, S. J., Gleeson, T., Wada, Y., Fawcett, P. J., Sharp, Z. D., McDonnell, J. J., and Welker, J. M.: The pronounced seasonality of global groundwater recharge, Water Resour. Res., 50, 8845–8867, https://doi.org/10.1002/2014WR015809, 2014.

Johnson, G. L. and Hanson, C. L.: Topographic and atmospheric influences on precipitation variability over a mountainous watershed, J. Appl. Meteor., 34, 68–86, 1995.

Kelleners, T. J., Chandler, D. G., McNamara, J. P., Gribb, M. M., and Seyfried, M. S.: Modeling Runoff Generation in a Small Snow-Dominated Mountainous Catchment, Vadose Zone J., 9, 517–527, https://doi.org/10.2136/vzj2009.0033, 2010.

Klos, P. Z., Link, T. E., and Abatzoglou, J. T.: Extent of the rain-snow transition zone in the western U.S. under historic and projected climate: Climatic rain-snow transition zone, Geophys. Res. Lett., 41, 4560–4568, https://doi.org/10.1002/2014GL060500, 2014.

Kormos, P. R., Marks, D., McNamara, J. P., Marshall, H. P., Winstral, A., and Flores, A. N.: Snow distribution, melt and surface water inputs to the soil in the mountain rain–snow transition zone, J. Hydrol., 519, 190–204, https://doi.org/10.1016/j.jhydrol.2014.06.051, 2014.

Kormos, P. R., Luce, C. H., Wenger, S. J., and Berghuijs, W. R.: Trends and sensitivities of low streamflow extremes to discharge timing and magnitude in Pacific Northwest mountain streams, Water Resour. Res., 52, 4990–5007, https://doi.org/10.1002/2015WR018125, 2016.

Kretchun, A. M., Scheller, R. M., Shinneman, D. J., Soderquist, B., Maguire, K., Link, T. E., and Strand, E. K.: Long term persistence of aspen in snowdrift-dependent ecosystems, Forest Ecology and Management, 462, 118005, https://doi.org/10.1016/j.foreco.2020.118005, 2020.

Leung, L. R., Qian, Y., Bian, X., Washington, W. M., Han, J., and Roads, J. O.: Mid-Century Ensemble Regional Climate Change Scenarios for the Western United States, Climatic Change, 62, 75–113, https://doi.org/10.1023/B:CLIM.0000013692.50640.55, 2004.

López-Moreno, J. I. and Stähli, M.: Statistical analysis of the snow cover variability in a subalpine watershed: Assessing the role of topography and forest interactions, J. Hydrol., 348, 379–394, https://doi.org/10.1016/j.jhydrol.2007.10.018, 2008.

Luce, C. H. and Holden, Z. A.: Declining annual streamflow distributions in the Pacific Northwest United States, 1948–2006, Geophys. Res. Lett., 36, L16401, https://doi.org/10.1029/2009GL039407, 2009.

MacNeille, R. B., Lohse, K. A., Godsey, S. E., Perdrial, J. N., and Baxter, C. N.: Influence of drying and wildfire on longitudinal chemistry patterns and processes of intermittent streams, Frontiers in Water, https://doi.org/10.3389/frwa.2020.563841, 2020.

Marks, D., Domingo, J., Susong, D., Link, T., and Garen, D.: A spatially distributed energy balance snowmelt model for application in mountain basins, Hydrol. Process., 13, 26, 1999.

Marks, D., Winstral, A., and Seyfried, M.: Simulation of terrain and forest shelter effects on patterns of snow deposition, snowmelt and runoff over a semi-arid mountain catchment, Hydrol. Process., 16, 3605–3626, https://doi.org/10.1002/hyp.1237, 2002.

Marks, D., Winstral, A., Reba, M., Pomeroy, J., and Kumar, M.: An evaluation of methods for determining during-storm precipitation phase and the rain/snow transition elevation at the surface in a mountain basin, Advances in Water Resources, 55, 98–110, https://doi.org/10.1016/j.advwatres.2012.11.012, 2013.

https://doi.org/10.5194/hess-2021-362
Preprint. Discussion started: 13 July 2021

Marshall, A. M., Link, T. E., Abatzoglou, J. T., Flerchinger, G. N., Marks, D. G., and Tedrow, L.: Warming Alters Hydrologic Heterogeneity: Simulated Climate Sensitivity of Hydrology-Based Microrefugia in the Snow-to-Rain Transition Zone, Water Resour. Res., 55, 2122–2141, https://doi.org/10.1029/2018WR023063, 2019.

McCabe, G. J. and Clark, M. P.: Trends and Variability in Snowmelt Runoff in the Western United States, J. Hydromet, 6, 476–482, https://doi.org/10.1175/JHM428.1, 2005.

McCabe, G. J., Wolock, D. M., Pederson, G. T., Woodhouse, C. A., and McAfee, S.: Evidence that Recent Warming is Reducing Upper Colorado River Flows, 21, 1–14, https://doi.org/10.1175/EI-D-17-0007.1, 2017.

McNamara, J. P., Chandler, D., Seyfried, M., and Achet, S.: Soil moisture states, lateral flow, and streamflow generation in a semi-arid, snowmelt-driven catchment, Hydrol. Process., 19, 4023–4038, https://doi.org/10.1002/hyp.5869, 2005.

Milly, P. C. D. and Dunne, K. A.: Colorado River flow dwindles as warming-driven loss of reflective snow energizes evaporation, Science, 367, 1252–1255, https://doi.org/10.1126/science.aay9187, 2020.

Molotch, N. P., Brooks, P. D., Burns, S. P., Litvak, M., Monson, R. K., McConnell, J. R., and Musselman, K.: Ecohydrological controls on snowmelt partitioning in mixed-conifer sub-alpine forests, Ecohydrol., 2, 129–142, https://doi.org/10.1002/eco.48, 2009.

Mott, R., Vionnet, V., and Grünewald, T.: The Seasonal Snow Cover Dynamics: Review on Wind-Driven Coupling Processes, Front. Earth Sci., 6, 197, https://doi.org/10.3389/feart.2018.00197, 2018.

Nash, J. E. and Sutcliffe, J. V.: River flow forecasting through conceptual models part I -A discussion of principles, J. Hydrol., 10, 282–290, 1970.

Nayak, A., Marks, D., Chandler, D. G., and Seyfried, M.: Long-term snow, climate, and streamflow trends at the Reynolds Creek Experimental Watershed, Owyhee Mountains, Idaho, United States, Water Resour. Res., 46, https://doi.org/10.1029/2008WR007525, 2010.

Naz, B. S., Kao, S.-C., Ashfaq, M., Rastogi, D., Mei, R., and Bowling, L. C.: Regional hydrologic response to climate change in the conterminous United States using high-resolution hydroclimate simulations, Global and Planetary Change, 143, 100–117, https://doi.org/10.1016/j.gloplacha.2016.06.003, 2016.

Nolin, A. W. and Daly, C.: Mapping "At Risk" Snow in the Pacific Northwest, J. Hydromet., 7, 1164–1171, https://doi.org/10.1175/JHM543.1, 2006.

Parr, C., Sturm, M., and Larsen, C.: Snowdrift Landscape Patterns: An Arctic Investigation, Water Resour. Res., 56, https://doi.org/10.1029/2020WR027823, 2020.

Patton, N. R., Lohse, K. A., Seyfried, M. S., Godsey, S. E., and Parsons, S. B.: Topographic controls of soil organic carbon on soil-mantled landscapes, Sci Rep, 9, 6390, https://doi.org/10.1038/s41598-019-42556-5, 2019.

Pflug, J. M. and Lundquist, J. D.: Inferring Distributed Snow Depth by Leveraging Snow Pattern Repeatability: Investigation Using 47 Lidar Observations in the Tuolumne Watershed, Sierra Nevada, California, 56, e2020WR027243, https://doi.org/10.1029/2020WR027243, 2020.

Pierson, F. B. and Cram, Z. K.: Reynolds Creek Experimental Watershed Runoff and Sediment Data Collection Field Manual, Northwest Watershed research Center, USDA-ARS, Boise, Idaho, 1998.

Pierson, F. B., Slaughter, C. W., and Cram, Z. K.: Monitoring Discharge and Suspended Sediment, Reynolds Creek Experimental Watershed, Idaho, USA, Northwest Watershed Research Center USDA-Agricultural Research Service, Boise, Idaho, 2000.

Planet Application Program Interface: In Space for Life on Earth. San Francisco, CA.: https://api.planet.com.

Pomeroy, J. W., Toth, B., Granger, R. J., Hedstrom, N. R., and Essery, R. L. H.: Variation in Surface Energetics during Snowmelt in a Subarctic Mountain Catchment, 4, 18, 2003.

Regonda, S. K., Rajagopalan, B., Clark, M., and Pitlick, J.: Seasonal Cycle Shifts in Hydroclimatology over the Western United States, 18, 372–384, https://doi.org/10.1175/JCLI-3272.1, 2005.

Schirmer, M., Wirz, V., Clifton, A., and Lehning, M.: Persistence in intra-annual snow depth distribution: 1. Measurements and topographic control, 47, https://doi.org/10.1029/2010WR009426, 2011.

Schweizer, J., Jamieson, J. B., and Schneebeli, M.: Snow avalanche formation, Rev. Geophys., 41, 1016, https://doi.org/10.1029/2002RG000123, 2003.

Seager, R., Naik, N., and Vogel, L.: Does Global Warming Cause Intensified Interannual Hydroclimate Variability?, J. of Climate, 25, 3355–3372, https://doi.org/10.1175/JCLI-D-11-00363.1, 2012.

Seyfried, M., Chandler, D., and Marks, D.: Long-Term Soil Water Trends across a 1000-m Elevation Gradient, Vadose Zone Journal, 10, 1276–1286, https://doi.org/10.2136/vzj2011.0014, 2011.

Seyfried, M. S., Grant, L. E., Marks, D., Winstral, A., and McNamara, J.: Simulated soil water storage effects on streamflow generation in a mountainous snowmelt environment, Idaho, USA, Hydrol. Process., 23, 858–873, https://doi.org/10.1002/hyp.7211, 2009.

Seyfried, M. S., Flerchinger, G. N., Bryden, S., Link, T. E., Marks, D. G., and McNamara, J. P.: Slope/Aspect Controls on Soil Climate: Field Documentation and Implications for Large-Scale Simulation of Critical Zone Processes, in review.

Shrestha, R. and Glenn, N. F.: 2007 Lidar-Derived Digital Elevation Model, Canopy Height Model and Vegetation Cover Model Data Sets for Reynolds Creek Experimental Watershed, Southwestern Idaho [Data set], https://doi.org/10.18122/B27C77, 2016.

Somers, L. D. and McKenzie, J. M.: A review of groundwater in high mountain environments, WIREs Water, 7, https://doi.org/10.1002/wat2.1475, 2020.

https://doi.org/10.5194/hess-2021-362
Preprint. Discussion started: 13 July 2021

Stephenson, G. R.: Soil-Geology_vegetation Inventories for Reynolds Creek Watershed, Agric. Exp. Stn. Univ. Idaho Coll. Agric., 1970.

Stewart, I. T.: Changes in snowpack and snowmelt runoff for key mountain regions, Hydrological Processes, 23, 78–94, https://doi.org/10.1002/hyp.7128, 2009.

Stewart, I. T., Cayan, D. R., and Dettinger, M. D.: Changes toward Earlier Streamflow Timing across Western North America, 18, 1136–1155, https://doi.org/10.1175/JCLI3321.1, 2005.

Sturm, M.: White water: Fifty years of snow research in WRR and the outlook for the future, Water Resour. Res., 51, 4948–4965, https://doi.org/10.1002/2015WR017242, 2015.

Sturm, M. and Wagener, A. M.: Using repeated patterns in snow distribution modeling: An Arctic example, 46, W12549, https://doi.org/10.1029/2010WR009434, 2010.

Tennant, C. J., Harpold, A. A., Lohse, K. A., Godsey, S. E., Crosby, B. T., Larsen, L. G., Brooks, P. D., Van Kirk, R. W., and Glenn, N. F.: Regional sensitivities of seasonal snowpack to elevation, aspect, and vegetation cover in western North America, Water Resour. Res., 53, 6908–6926, https://doi.org/10.1002/2016WR019374, 2017.

Trujillo, E., Ramírez, J. A., and Elder, K. J.: Topographic, meteorologic, and canopy controls on the scaling characteristics of the spatial distribution of snow depth fields: SPATIAL SCALING OF SNOW DEPTH, Water Resour. Res., 43, https://doi.org/10.1029/2006WR005317, 2007.

Trujillo, E., Havens, S., Hedrick, A. R., Johnson, M., Robertson, M., Pierson, F. B., and Marks, D. G.: Utilizing spatially resolved SWE to inform snowfall interpolation across a headwater catchment in the Sierra Nevada, C33B-1579, https://doi.org/bib code: 2019AGUFM.C33B1579T, 2019.

Viviroli, D., Dürr, H. H., Messerli, B., Meybeck, M., and Weingartner, R.: Mountains of the world, water towers for humanity: Typology, mapping, and global significance, Water Resources Research, 43, https://doi.org/10.1029/2006WR005653, 2007.

Vögeli, C., Lehning, M., Wever, N., and Bavay, M.: Scaling Precipitation Input to Spatially Distributed Hydrological Models by Measured Snow Distribution, Front. Earth Sci., 4, https://doi.org/10.3389/feart.2016.00108, 2016.

Wang, R., Kumar, M., and Marks, D.: Anomalous trend in soil evaporation in a semi-arid, snow-dominated watershed, Advances in Water Resources, 57, 32–40, https://doi.org/10.1016/j.advwatres.2013.03.004, 2013.

Westerling, A. L., Hidalgo, H. G., Cayan, D. R., and Swetnam, T. W.: Warming and Earlier Spring Increase Western U.S. Forest Wildfire Activity, Science, 313, 940–943, https://doi.org/10.1126/science.1128834, 2006.

Williams, C. J., McNamara, J. P., and Chandler, D. G.: Controls on the temporal and spatial variability of soil moisture in a mountainous landscape: the signature of snow and complex terrain, Hydrology and Earth System Sciences, 13, 1325–1336, https://doi.org/10.5194/hess-13-1325-2009, 2009.

https://doi.org/10.5194/hess-2021-362
Preprint. Discussion started: 13 July 2021

Winstral, A. and Marks, D.: Simulating wind fields and snow redistribution using terrain-based parameters to model snow accumulation and melt over a semi-arid mountain catchment, Hydrol. Process., 16, 3585–3603, https://doi.org/10.1002/hyp.1238, 2002.

Winstral, A. and Marks, D.: Long-term snow distribution observations in a mountain catchment: Assessing variability, time stability, and the representativeness of an index site, Water Resour. Res., 50, 293–305, https://doi.org/10.1002/2012WR013038, 2014.

https://doi.org/10.5194/hess-2021-362
Preprint. Discussion started: 13 July 2021

Tables

Table 1. Precipitation, discharge and SWI characteristics for each water year including: total precipitation (mm), the fraction of precipitation falling as snow (snowfall fraction), dates of the start ($snow_{start}$) and end ($snow_{end}$) of the snowy season, defined as > 1 cm of snow at weather station jdt124b (except for 2005, for which only data for weather station jdt125 was available), dates at which the simulated snow cover had melted (melt-out date; SCA = 0), annual discharge (Q_{annual}) and runoff efficiency (Q_{annual}/SWI_{avg}) as well as the start ($Flow_{start}$) and end ($Flow_{end}$) of surface flow at the catchment outlet, and simulated surface water inputs (SWI). We report the catchment-average SWI (SWI_{avg}) as well as SWI from rain (SWI_{rain}), SWI from snow (SWI_{snow}), the 98th percentile of SWI (SWI_{98}), maximum SWI (SWI_{max}) and the average SWI for north-facing slopes (excluding the drift area, $SWI_{NF\text{-}drift}$) and south-facing slopes (SWI_{SF})

WY		2005 Rainy	2009 Lidar available	2010 Snowy	2011 Wet	2014 Dry
Precipitation	mm	542	549	531	693	450
Snowfall fraction	-	0.23	0.49	0.57	0.41	0.30
$Snow_{start}$	dd-mon (DOWY)	16-Oct* (16)	01-Nov (32)	04-Oct (4)	06-Nov (37)	20-Oct (20)
$Snow_{end}$	dd-mon (DOWY)	01-Mar* (152)	19-Apr (201)	26-May (238)	01-May (213)	06-Apr (188)
SCA = 0	dd-mon (DOWY)	02-Jun (245)	14-Jun (257)	16-Jun (259)	18-Jun (261)	14-May (226)
Q_{annual}	mm	62	81	117	307	80
Q/SWI_{avg}	-	0.11	0.14	0.21	0.46	0.16
$Flow_{start}$	dd-mon (DOWY)	11-Nov (38)	22-Nov (54)	12-Nov (43)	24-Oct (24)	28-Oct (28)
$Flow_{end}$	dd-mon (DOWY)	25-Aug (328)	25-Aug (328)	26-Aug (329)	-	13-Jul (285)
SWI_{avg}	mm	557	587	553	672	506
SWI_{rain}	mm	145	271	310	229	170
SWI_{snow}	mm	412	316	243	443	336
SWI_{98}	mm	982	1394	1513	1588	1015
SWI_{max}	mm	2005	3350	3863	3892	2219
$SWI_{NF\text{-}drift}$	mm	551	568	534	665	490
SWI_{SF}	mm	505	456	407	556	430

***dates based on measurements at jdt125 (outlet) rather than 124b (close to top of the catchment, see Fig. 1)**

https://doi.org/10.5194/hess-2021-362
Preprint. Discussion started: 13 July 2021

Hydrology and Earth System Sciences
Discussions
Open Access
EGU

Table 2. Nash-Sutcliffe Efficiency's (NSE; Nash and Sutcliffe, 1970) and root mean square errors (RMSE, cm) for simulated and observed snow depths at each weather station, as well as NSE for the normalized (z-transformed) snow depths (NSE_{norm}). Dashes (-) indicate that no observed snow depths were available in that year. See Supplement S4 for the time series of observed and simulated snow depths.

		Outlet	North-facing				South-facing			Upper region		Median
	Station	jd125	jdt1	jdt2	jdt3	jdt4	jdt2b	jdt3b	jdt4b	jdt5	jd124b	
NSE	**2005**	0.83	-	-	-	-	-	-	-	-	-	0.83
	2009	0.45	0.67	0.09	0.95	0.91	-	-	-	0.65	0.84	0.67
	2010	0.01	0.92	0.91	0.68	0.86	-	-	-	0.67	0.92	0.86
	2011	0.40	-0.46	0.63	0.03	-9.60	0.52	0.76	0.54	-0.06	-5.56	0.22
	2014	0.80	-2.07	0.76	0.49	0.25	0.39	0.60	0.80	0.81	0.66	0.63
NSE_{norm}	**2005**	0.87	-	-	-	-	-	-	-	-	-	0.87
	2009	0.65	0.50	0.50	0.83	0.85	-	-	-	0.89	0.97	0.83
	2010	0.25	0.94	0.92	0.96	0.95	-	-	-	0.68	0.94	0.94
	2011	0.86	0.34	0.73	0.89	-0.86	0.55	0.75	0.67	0.63	0.15	0.65
	2014	0.77	0.59	0.75	0.81	0.64	0.33	0.64	0.72	0.80	0.79	0.74
RMSE (cm)	**2005**	0.8	-	-	-	-	-	-	-	-	-	0.8
	2009	11.5	9.7	19.1	5.11	7.9	-	-	-	11.1	9.1	9.7
	2010	11.7	3.7	5.1	11.1	9.3	-	-	-	8.7	5.6	8.7
	2011	2.9	5.5	4.2	8.3	30.3	2.1	2.1	1.9	5.0	15.0	4.6
	2014	1.2	5.7	2.0	3.6	4.7	1.9	2.2	1.1	1.6	2.4	2.1

Figures

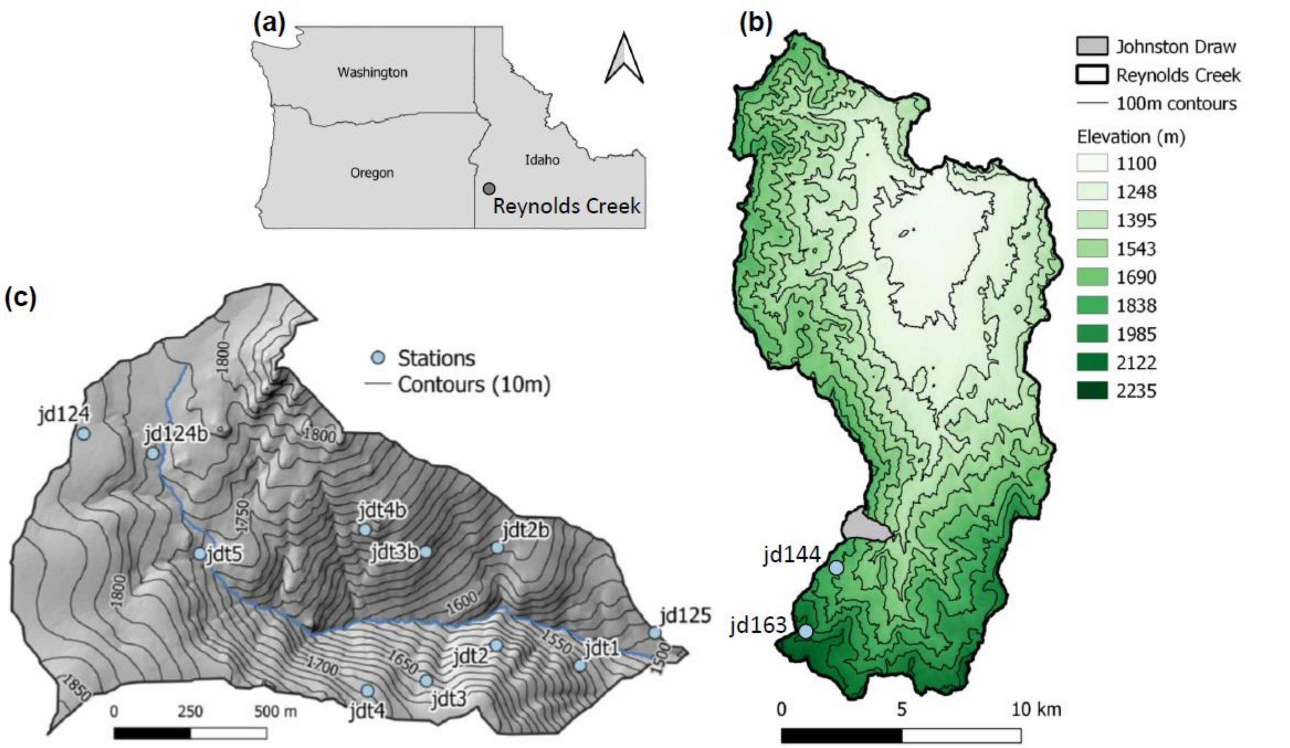

Fig. 1 Maps of the location of (a) the Reynolds Creek Experimental Watershed (RCEW) in the state of Idaho (USA), (b) Reynolds Creek Experimental Watershed with indication of elevation (white = lower, dark green = higher), 100 m contour lines, the location of Johnston Draw (grey polygon) and two additional precipitation gauges (dots) indicated in light blue, and (c) Johnston Draw with the weather stations (light blue dots), stream (blue line), and 10 m contour lines (black lines), overlain on a hillshade DEM.

https://doi.org/10.5194/hess-2021-362
Preprint. Discussion started: 13 July 2021

Hydrology and Earth System Sciences
Discussions

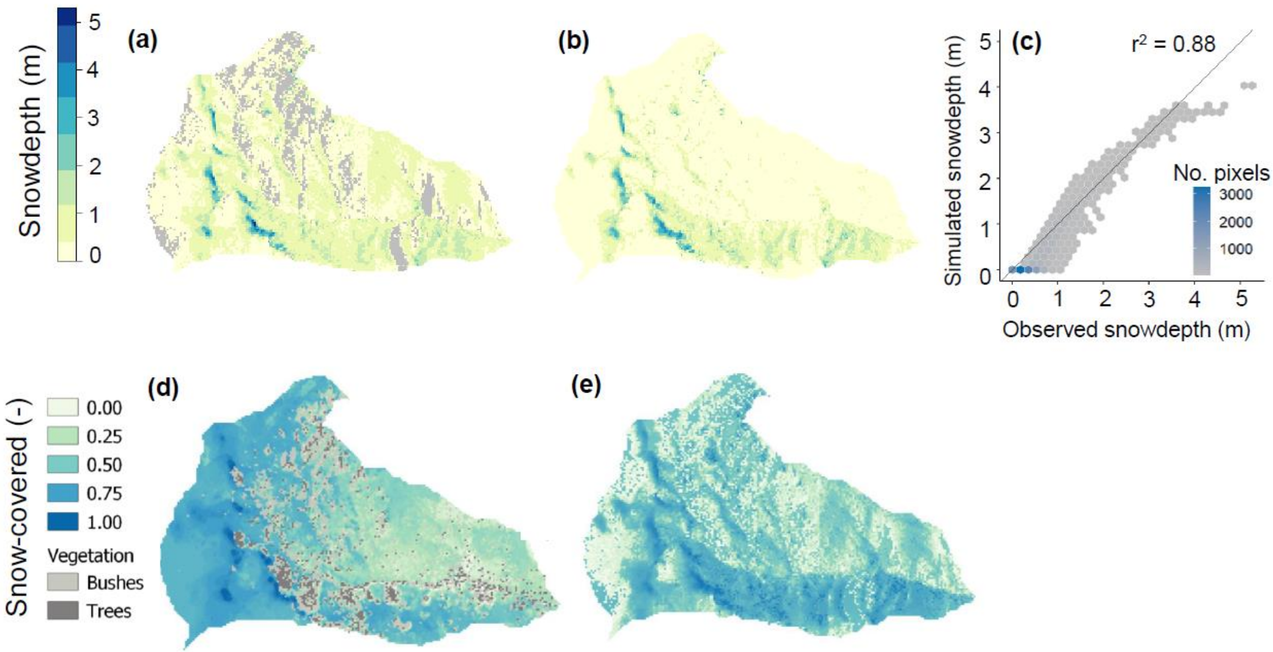

Fig. 2. (a) Lidar snow depth (m) at 3-m resolution on 18 March 2009, and (b) simulated snow depth for the same day, where yellow indicates low snow depths, blue high snow depths, and grey the areas for which the snow depth could not reliably be determined from the lidar measurement (see section 3.2). (c) shows a hexagonal bin plot comparing the observed and simulated snow depths with grey colors indicating fewer pixels and blue indicating more pixels included per bin. (d) shows the fraction of images for which sites were snow-covered, using 3-m resolution satellite imagery for the available images (n=41) of water year 2019 (see section 3.2), and (e) shows the fraction of time during which each pixel was snow-covered, using the simulated snow cover from the beginning of the water year 2009 until all snow had melted (n=238). Bushes and trees (marked in grey in D) inhibited the exact determination of the snow cover for the satellite imagery in some locations.

https://doi.org/10.5194/hess-2021-362
Preprint. Discussion started: 13 July 2021

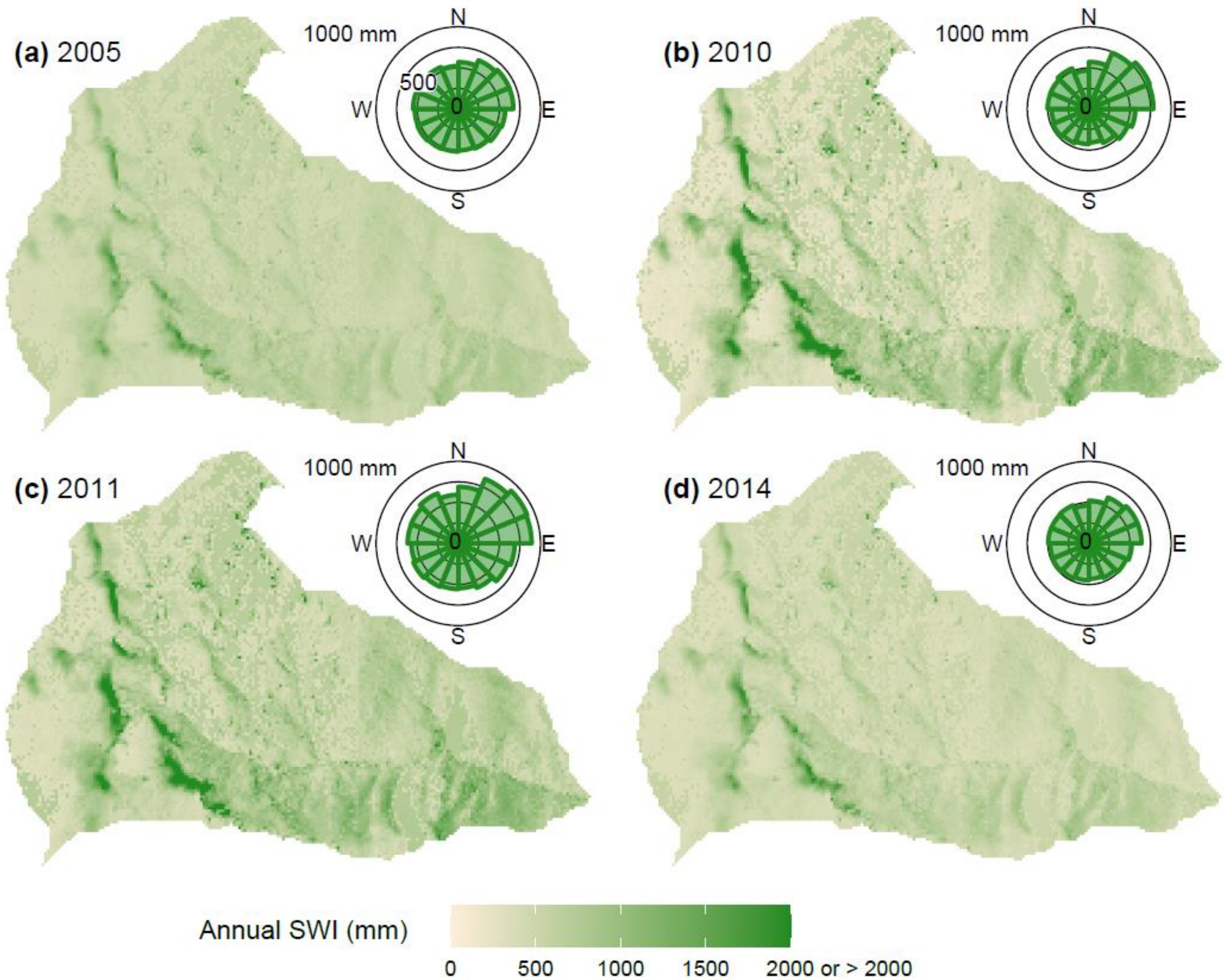

Fig. 3. Maps showing the yearly sum of surface water inputs (SWI, mm) for (a) rainy 2005, (b) snowy 2010, (c) wet 2011 and (d) dry 2014, with polar diagram insets showing the average sum of SWI per 10-m grid cell for each aspect (binned per 22.5°). Higher SWI values are shown in darker colours, lower SWI values in lighter colours, and SWI values are capped at 2000 mm to enhance the contrast. Maximum annual SWI values are shown in Table 1 and a map of simulated SWI for 2009 is shown in Supplement S5.

https://doi.org/10.5194/hess-2021-362
Preprint. Discussion started: 13 July 2021

Hydrology and Earth System Sciences
Open Access
Discussions

693
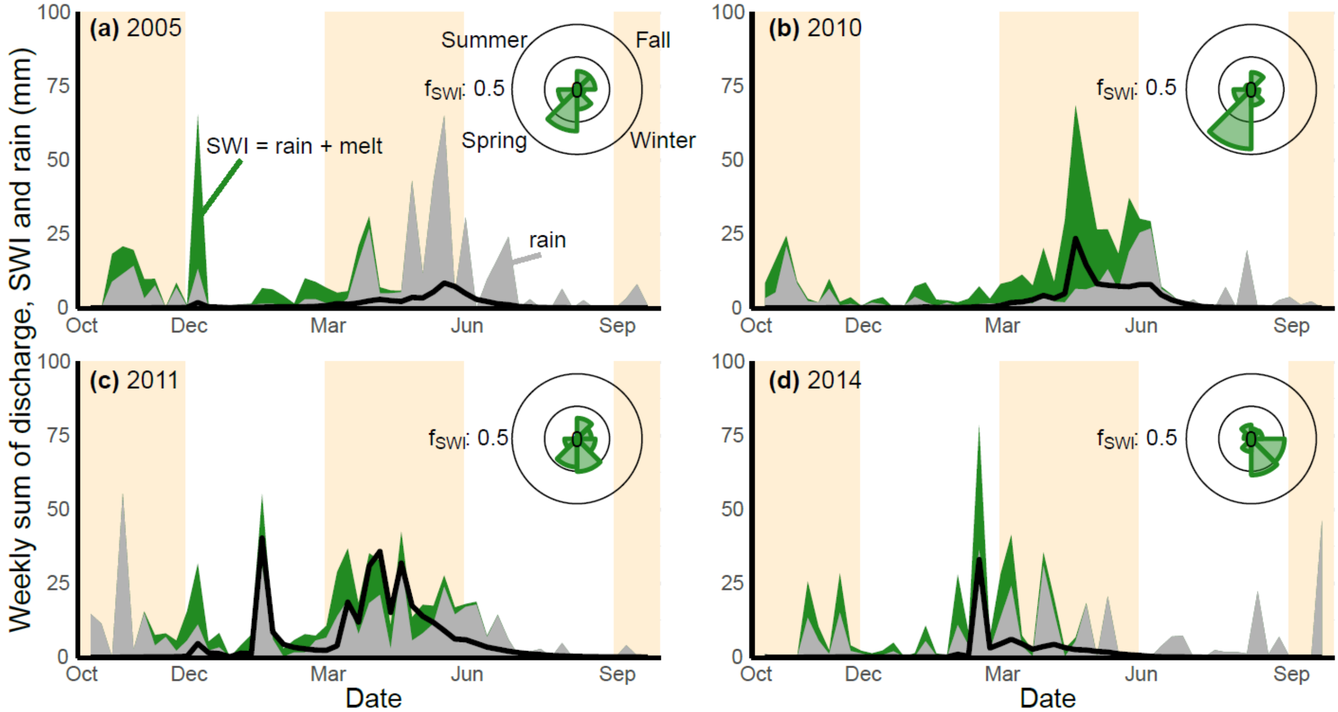

694 **Fig. 4 Weekly sums of surface water inputs (SWI, summation of rainfall and snowmelt, green polygons, mm), rainfall**
695 **(grey polygons, mm) and specific discharge (black line graph, mm) for (a) rainy 2005, (b) snowy 2010, (c) wet 2011 and**
696 **(d) dry 2014. Background panels are coloured according to the different seasons (fall, winter, spring, summer, fall).**
697 **The polar diagram insets indicate which fraction of SWI (f_{SWI}) occurred in which season.**
698

https://doi.org/10.5194/hess-2021-362
Preprint. Discussion started: 13 July 2021

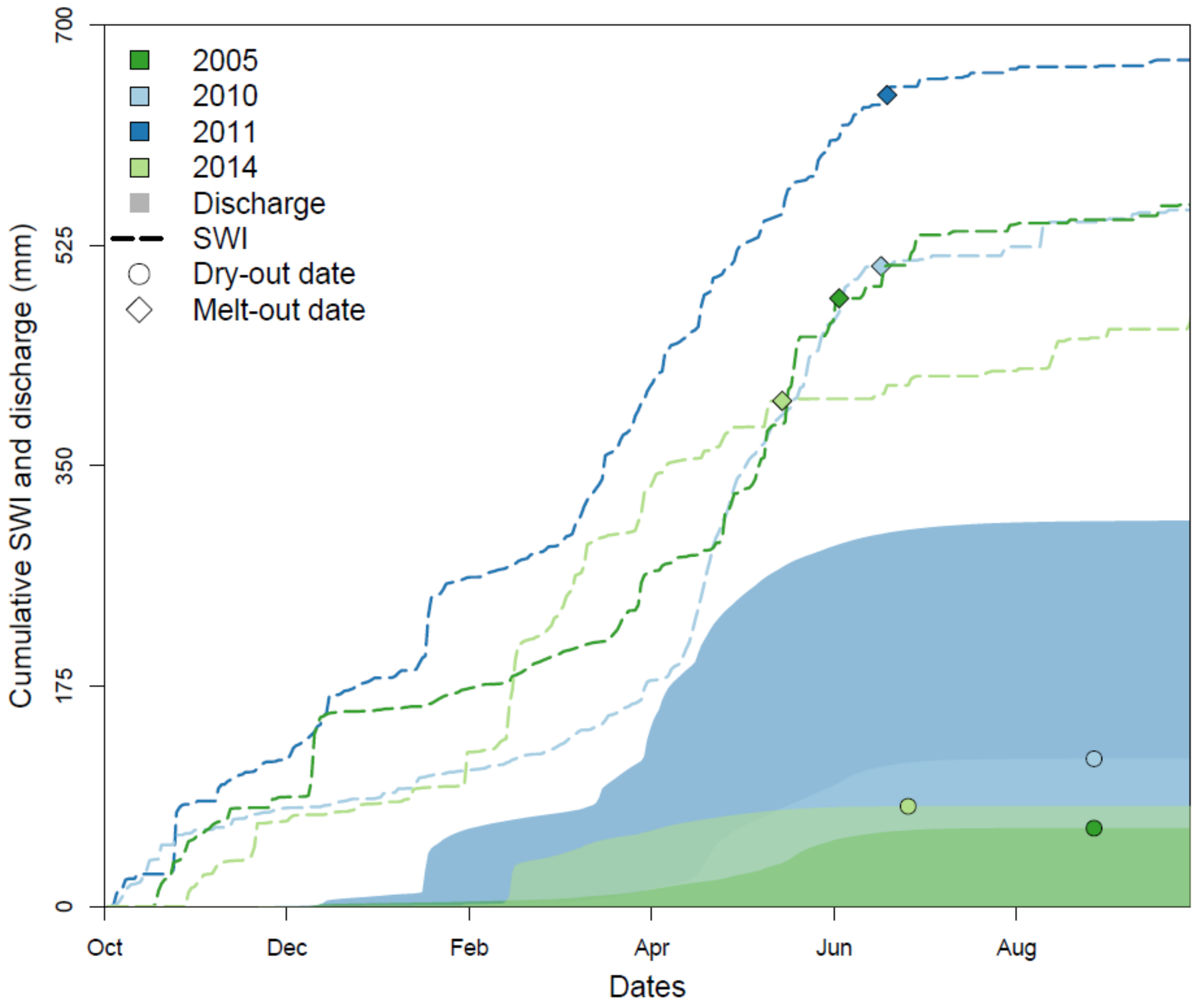

Fig. 5 Cumulative surface water inputs (SWI, dashed lines, mm) and discharge (coloured polygons, mm) for each of the water years (dark green = rainy 2005, light blue = snowy 2010, dark blue = wet 2011, light green = dry 2014). Circles indicate the day at which the stream ceased to flow at the catchment outlet (dry-out date, please note that the stream did not cease to flow in 2011) and diamonds indicate the day at which all snow had melted from the catchment (melt-out date).

Hydrology and Earth System Sciences
Discussions

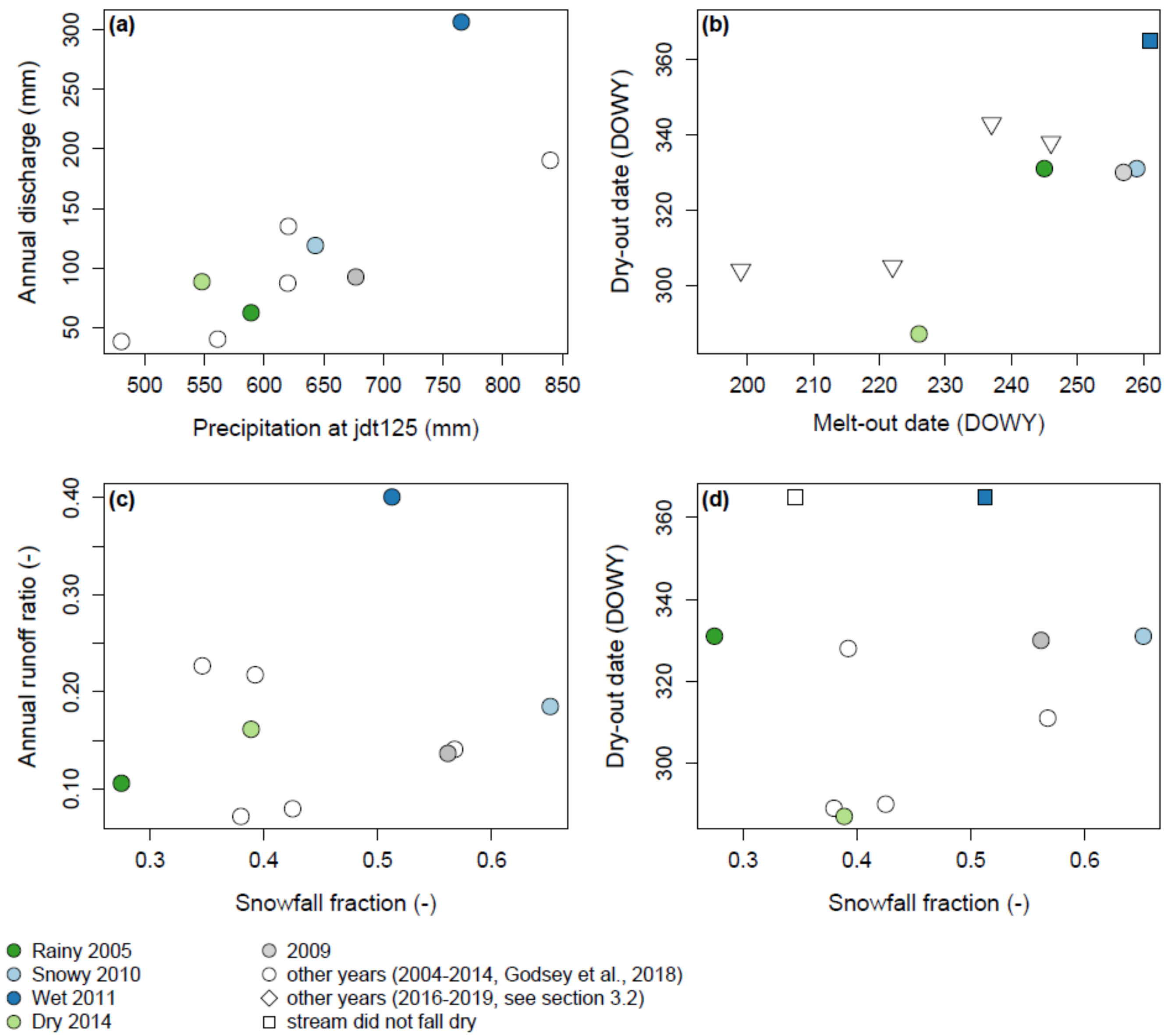

Fig. 6 Scatter plots of (a) annual discharge at the catchment outlet (mm) and annual precipitation at the lowest precipitation gauge (jdt125, mm), (b) the day that surface flow in the stream ceased (dry-out date, day of water year (DOWY)) and the day on which all snow had melted (melt-out date, DOWY), (c) annual runoff ratio (annual discharge/annual precipitation at jdt125) and the annual snowfall fraction (-), and (d) the stream dry-out date and the annual snowfall fraction. Years in which the stream did not fall dry are projected to the last day of the hydrological year. R^2 and p-values for linear regressions between the variables in each panel are: (a) r^2=0.60, p-value=0.005, (b) r^2=0.48, p-value=0.023, (c) r^2=-0.09, p-value=0.607, (d) r^2=-0.11, p-value=0.790.